Comparison of two depth-averaged numerical models for debris flow runout estimation

NRC Research Press

ARTICLE

Comparison of two depth-averaged numerical models for debris flow runout estimation

Federico Vagnon, Marina Pirulli, Angel Yague, and Manuel Pastor

Abstract: This paper analyses an important aspect of the continuum numerical modelling of rapid landslides as debris flows: "By using the same rheological parameter values, are the results obtained with codes that implement the same constitutive equations, but a different numerical solver, equal?" To answer this question, the two numerical codes RASH3D and GeoFlow_SPH are used here to back-analyse the debris flow event that occurred in the Nora stream (northwestern Italian Alps) in October 2000. Comparison of results evidenced that the RASH3D best-fit rheological values for the Nora event back-analysis overestimated both the final depositional heights and the simulated flow velocities if used in GeoFlow_SPH. To obtain thickness values comparable with those measured in situ, it was necessary to re-calibrate GeoFlow_SPH rheological parameter values. This way, with the exception of a larger lateral spreading of the sliding mass given by RASH3D, both thickness and velocity values were similar for the two numerical codes.

Key words: debris flow, runout estimation, RASH3D code, GeoFlow_SPH code, continuum numerical modelling.

Résumé : Cet article analyse un aspect important de la modélisation numérique continue des glissements rapides en tant que coulées de débris : « En utilisant les mêmes valeurs de paramètres rhéologiques, les résultats, obtenus avec des codes qui mettent en œuvre les mêmes équations constitutives, mais un solveur numérique différent, sont-ils égaux? » Pour répondre à cette question, les deux codes numériques RASH3D et GeoFlow_SPH sont utilisés ici pour rétro-analyser l'événement de coulée de débris survenu dans le ruisseau Nora (Alpes italiennes du nord-ouest) en octobre 2000. La comparaison des résultats a montré que les valeurs rhéologiques les mieux ajustées par RASH3D pour la rétro-analyse de l'événement Nora surestimaient à la fois les hauteurs de dépôt finales et les vitesses d'écoulement simulées si elles étaient utilisées dans GeoFlow_SPH. Afin d'obtenir des valeurs d'épaisseur comparables à celles mesurées in situ, il a fallu refaire le calage des valeurs des paramètres rhéologiques de GeoFlow_SPH. Ainsi, à l'exception d'un plus grand étalement latéral de la masse glissante donné par RASH3D, les deux valeurs d'épaisseur et de vitesse étaient similaires pour les deux codes numériques. [Traduit par la Rédaction]

Mots-clés : coulée de débris, estimation de la dérive, code RASH3D, code GeoFlow_SPH, modélisation numérique continue.

1. Introduction

Every year thousands of landslides all over the world cause loss of human lives and enormous economic damages. These phenomena remind us of our society's vulnerability to natural disasters (Jakob and Hungr 2005).

In recent decades, climate changes have increased the probability of occurrence of a particular type of landslide: debris flow. Glacier melting, permafrost degradation, and increase of extreme (short and intense) rainfall are triggering factors for this dangerous and destructive phenomenon. The main characteristics of debris flows are their unpredictability, their high velocity, and their long travel distances.

Because their potential for destruction usually cannot practically be reduced by stabilization of the source area (Hungr 1995), engineering risk analyses are required, including prediction of runout parameters (maximum travel distance reached, flow velocities, thickness and distribution of the deposit). As it is very difficult to obtain data from monitoring of real events and to apply statistical methods, other methodologies for evaluating flow characteristics are required. Numerical models represent a useful tool for investigating, within realistic geological contexts, the dynamics of these events.

Existing models can be divided into two main groups: those that follow empirical approaches and those that are based on dynamic numerical models (continuum or discontinuum). Empirical models, based on correlation among historical data (e.g., Cannon 1993; Corominas 1996; Rickenmann 1999), are more practical and easy to use, but they should only be applied to conditions similar to those on which their development are based (Rickenmann 2005).

Alternatively, dynamic numerical models are viable tools for forecasting flow parameters (e.g., Savage and Hutter 1989; O'Brien et al. 1993; Hungr 1995; Iverson and Denlinger 2001; McDougall and Hungr 2004; Pirulli 2005; Pastor et al. 2009). In particular, the basic concept of continuum-based methods is that the release mass dynamics can be described in terms of flow-like behaviour. The moving mass can entrain additional material from the path and eventually deposits, when it reaches slopes that are sufficiently flat. Whatever code is used, the choice of the rheological law, the terrain characteristics, and the presence of erosion–deposition areas affect the results (Pirulli and Marco 2010). Consequently, these methods require an accurate calibration of parameters on the basis of back-

Received 2 August 2017. Accepted 16 April 2018.

F. Vagnon. Department of Earth Science, University of Torino, Via Valperga Caluso 35, 10125 Turin, Italy.
M. Pirulli. Department of Structural, Geotechnical and Building Engineering, Politecnico di Torino, Corso Duca degli Abruzzi 24, 10129 Turin, Italy.
A. Yague and M. Pastor. Department of Applied Mathematics and Computer Science, ETSI Caminos, Canales y Puertos, Universidad Politécnica de Madrid (UPM), Madrid, Spain.
Corresponding author: Federico Vagnon (email: fvagnon@unito.it).

analysis of real events for assessing and forecasting potential dangerous areas.

Another important issue is the choice of the most suitable simulation code: Pirulli and Sorbino (2008) stated that the use of more than one code for simulating debris flow events is recommended to compare runout results, providing and highlighting the main differences. This aspect is particularly important because it helps users in the decisional process in assessing potential risks and evaluating–designing possible countermeasures.

The purpose of this paper is to investigate if codes that implement the same governing equations, but with fundamentally different numerical solvers, produce different results, when the same rheological law and rheological values are used to model a given case, and the extent to which obtained results may differ. This is an important aspect and it should be taken into account by the engineers (e.g., in the design of structural countermeasures and mapping of dangerous areas). Because one of the main functions of the numerical codes should be to forecast future events and to predict their effects, their choice becomes, for engineers, an important aspect to take into account (Vagnon 2017).

In the following sections, the two different continuum-based codes RASH3D (Pirulli 2005) and GeoFlow_SPH (Pastor et al. 2009, 2015) are briefly described and used to back-analyse a real debris flow event that occurred in northern Italy. The obtained results are compared and discussed.

2. Continuum mechanics modelling

To apply continuum mechanics to flow-like landslide modelling implies that both characteristic thickness (H) and length (L) of the flowing mass are assumed to exceed the size of single moving particles in the order of several times. With this hypothesis, the real moving mixture, composed of solid and fluid phases, can be replaced by an "equivalent fluid", whose properties have to approximate the bulk behaviour of the real mixture.

Furthermore, a kinematic boundary condition is imposed on free and bed surfaces according to which mass neither enters nor leaves at these two surfaces unless an erosion law is introduced.

Under the aforementioned conditions and assuming that the sliding mass is described as a single-phase, incompressible, and homogeneous material (Savage and Hutter 1989; Hungr 1995; Iverson and Denlinger 2001), the motion can be described using the balance of mass and momentum equations:

$$\nabla \cdot \boldsymbol{v} = 0 \tag{1}$$

$$\rho\left(\frac{\partial \boldsymbol{v}}{\partial t} + \boldsymbol{v}\cdot\nabla\boldsymbol{v}\right) = -\nabla\cdot\boldsymbol{\sigma} + \rho\boldsymbol{g} \tag{2}$$

where $\boldsymbol{v}$ denotes the three-dimensional velocity vector (= (v_x, v_y, v_z)) inside the mass in an (x, y, z) coordinate system that will be discussed later, $\boldsymbol{\sigma}(x, y, z, t)$ is the Cauchy stress tensor, ρ is the mass density, and $\boldsymbol{g}$ is the vector of gravitational acceleration.

Depth averaging of these equations and shallow flow assumption require the choice of an appropriate coordinate system. During the flow, the characteristic thickness (H) of the flow is considerably smaller than its extent parallel to the bed (L). In the case of significant slopes, the shallow flow assumption is more significant in a reference frame linked to the topography and the classical shallow water approximation relating horizontal and vertical direction is not appropriate (Mangeney-Castelnau et al. 2003). As in the work by Iverson and Denlinger (2001), the equations are here written in terms of a local, orthogonal Cartesian coordinate system in which the z coordinate is normal to the local topography.

In the reference frame linked to the topography, equations of mass and momentum in the x and y direction derived by integration of Navier–Stokes eqs. (1) and (2) read

$$\begin{cases} \dfrac{\partial h}{\partial t} + \dfrac{\partial(\bar{v}_x h)}{\partial x} + \dfrac{\partial(\bar{v}_y h)}{\partial y} = 0 \\ \rho\left[\dfrac{\partial(\bar{v}_x h)}{\partial t} + \dfrac{\partial\left(\bar{v}_x^2 h\right)}{\partial x} + \dfrac{\partial(\bar{v}_x \bar{v}_y h)}{\partial y}\right] = \mp\dfrac{\partial(\bar{\sigma}_{xx} h)}{\partial x} + \dfrac{\partial(\bar{\sigma}_{xy} h)}{\partial y} + T_{x_{(z=b)}} + \rho g_x h \\ \rho\left[\dfrac{\partial(\bar{v}_y h)}{\partial t} + \dfrac{\partial(\bar{v}_y \bar{v}_x h)}{\partial x} + \dfrac{\partial\left(\bar{v}_y^2 h\right)}{\partial y}\right] = +\dfrac{\partial(\bar{\sigma}_{xy} h)}{\partial x} \mp \dfrac{\partial(\bar{\sigma}_{yy} h)}{\partial y} + T_{y_{(z=b)}} + \rho g_y h \end{cases} \tag{3}$$

where $\bar{\boldsymbol{v}}$ denotes the depth-averaged flow velocity (= $(\bar{v}_x, \bar{v}_y)$); h is the flow depth; T_x and T_y are the traction vector components in the x and y directions, respectively; b is the bottom elevation in the (x, y, z) coordinate system; and g_x, g_y are the projections of the gravity vector along the x and y directions, respectively. The traction vector $\boldsymbol{T} = (T_x, T_y, T_z) = -\boldsymbol{\sigma}\cdot\boldsymbol{n}_b$, where $\boldsymbol{n}_b$ is the unit vector normal to the bed, and

$$\boldsymbol{T} = \begin{pmatrix} \sigma_{xx}\dfrac{\partial b}{\partial x} + \sigma_{xy}\dfrac{\partial b}{\partial y} - \sigma_{xz} \\ \sigma_{xy}\dfrac{\partial b}{\partial x} + \sigma_{yy}\dfrac{\partial b}{\partial y} - \sigma_{yz} \\ \sigma_{xz}\dfrac{\partial b}{\partial x} + \sigma_{yz}\dfrac{\partial b}{\partial y} - \sigma_{zz} \end{pmatrix}_b$$

A scale analysis with respect to H/L (Gray et al. 1999; Mangeney-Castelnau et al. 2003) leads to neglecting the acceleration normal to the topography and the horizontal gradients of the stresses in the z equation, leading to $\sigma_{zz} = \rho g_z(h - z)$. The normal traction reduced to $T_z = -\sigma_{zz|b}$ and $(\partial/\partial x_i)(h\bar{\sigma}_{xy})$ can be neglected in the z and y depth-averaged momentum equations.

Depth-averaged integration simplifies the three-dimensional description of the flow, but the vertical velocity distribution is lost and replaced with a single average velocity value in the flow depth for each point of the flowing mass. Furthermore, the rheological characteristics are included in a single term acting at the interface between flow and terrain surface.

In 1989 depth-averaged equations were applied for the first time to the analysis of propagation of a granular mass by Savage and Hutter; since then, many numerical models were progressively implemented. Even if based on the same balance equations and the same simplifying hypotheses, the aforementioned codes mainly differ for the adopted numerical solver.

In the following sections, the characteristics and peculiarity of the two continuum numerical codes, RASH3D (Pirulli 2005) and GeoFlow_SPH (Pastor et al. 2009, 2015), are presented, focusing on both similarities and main differences.

3. RASH3D versus GeoFlow_SPH

In continuum dynamics, the equations of motion can be formulated in one of two frames of reference: Eulerian or Langrangian. A Eulerian reference frame is fixed in space, while a Lagrangian reference frame moves with the flow. Furthermore, to perform the mass balance calculation, a discretization of the equations has to be made by using a mesh (structured or unstructured) or a meshless approach. In a meshless scheme, in lieu of a mesh, balance is determined from the spatial distribution of a number of moving reference masses (known as particles). The RASH3D and GeoFlow_SPH codes adopt the first and the second discretization-approach, respectively. In particular, RASH3D discretizes the terrain on a general triangular grid with a finite element data structure and it computes the flow in the different flow directions using a particular control volume; whereas, in GeoFlow_SPH, the sliding soil is schematized as a series of nodes with fictitious moving mass and pressure terms. That is, RASH3D uses a Eulerian method and a fixed reference system for evaluating flow motion characteristics (for each node of the mesh, velocity and thickness and their evolution in time are calculated). In contrast, GeoFlow_SPH uses a meshless Langrangian method known as smoothed particle

Fig. 1. Triangular finite-element mesh for dual cell C_i (adapted from Mangeney-Castelnau et al. 2003). n_{ij}, normal vector to Γ_{ij} directed from P_i to P_j, one of mesh vertexes that surround P_i; Γ_{ij}, boundary of dual cell C_i separating P_i from P_j.

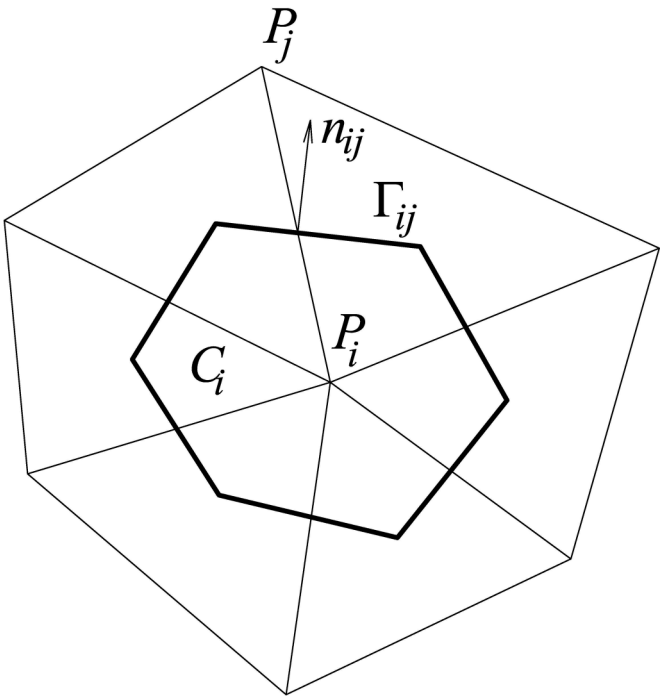

Fig. 2. Nodes and numerical integration on smoothed particle hydrodynamics (SPH) mesh (Pastor et al. 2009). [Colour online.]

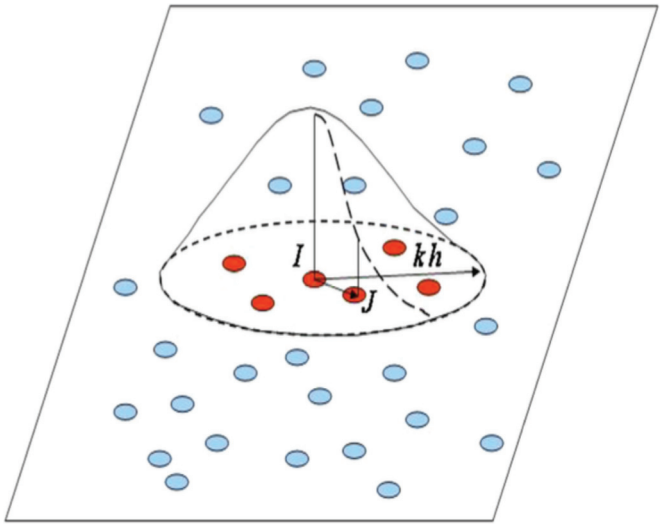

hydrodynamics (SPH) and the reference system is integral with the particle position.

Both these codes are based on a depth-average continuum mechanics based approach and they need as input data to run an analysis: (*i*) the pre-event digital elevation model (DEM), (*ii*) the position and the magnitude of a source area, and (*iii*) the rheological law.

A relation deduced from the mechanical behaviour of the material has to be imposed between the tangential stress T_t (= (T_x, T_y)) and $\boldsymbol{v}$ and h to close the equations forming eq. (3). The depth-averaged mass is then considered as an effective material submitted to an empirical friction introduced in the tangential traction term T_t (Pouliquen 1999).

Fig. 3. One-dimensional (1D) dam break problem over dry bed. [Colour online.]

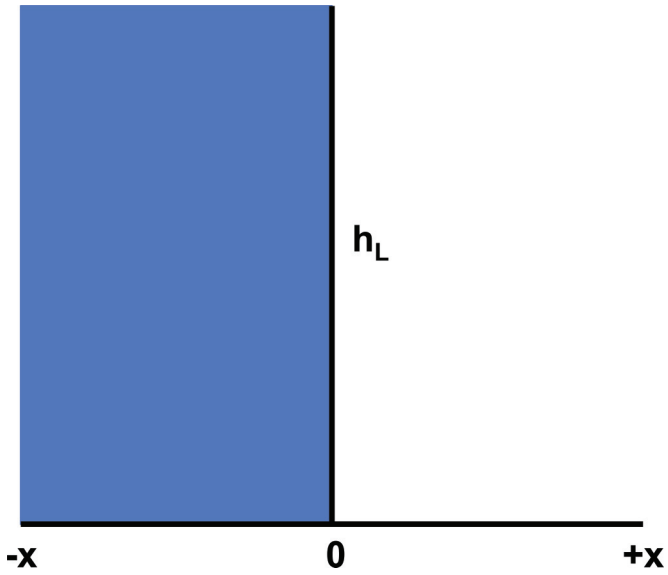

Considering a Coulomb-type friction law, the norm of the tangential traction $\|T_t\|$ at the bed is related to the norm of the normal traction $\|T_n\| = |T_z| = |\sigma_{zz|b}|$ at the bed, through a friction coefficient μ; that is, $\|T_t\| \leq \sigma_c = \mu\|T_n\| = \mu\rho g_z h$ and acting opposite to the velocity (i.e., $T_i = -\mu\rho g_z h(\overline{\boldsymbol{v}}_i/\|\overline{\boldsymbol{v}}\|)$). The value of σ_c defines the upper bound of the admissible stresses.

Similarly, the Voellmy rheology gives

$$T_i = -\left(\rho g_z h\mu + \frac{\rho \mathbf{g}\overline{\boldsymbol{v}}_i^2}{\xi}\right)\frac{\overline{\boldsymbol{v}}_i}{\|\overline{\boldsymbol{v}}\|} \qquad i = (x, y) \tag{4}$$

where μ is the frictional coefficient equal to the tangent of the bulk basal friction angle and ξ is the turbulent coefficient.

The Voellmy rheology, as stated by many authors (e.g., Hungr and Evans 1996; Rickenmann and Koch 1997; Revellino et al. 2004; Pirulli 2009), produces most consistent results in terms of debris spreading and distribution as well as velocity data when debris flows are analysed. This is why it has been selected for comparing the two codes results in the case of the Rio Nora debris flow event.

It is finally underlined that the two selected codes have been widely validated through the back-analysis of laboratory experiments (e.g., Manzella et al. 2008; Pisani et al. 2013; Sauthier et al. 2015) and of real events (e.g., Pirulli 2009, 2016; Pirulli and Marco 2010; Pirulli and Pastor 2012; Cascini et al. 2014; Cuomo et al. 2014; Pastor et al. 2014; Dutto et al. 2017; Pirulli et al. 2017), and in the frame of a common benchmark exercise (see Pastor et al. 2007; Pirulli and Scavia 2007).

3.1. RASH3D code

The RASH3D code, developed by Pirulli (2005) is an upgrade for modelling landslide run out problems of a pre-existing numerical code (SHWCIN) developed by Audusse et al. (2000) using a finite volume method.

This type of method requires the formulation of the equations in terms of conservation laws.

The system of equations shown as eq. (3), approximated in accordance with the scale analysis described in Section 2 “Continuum mechanics modelling”, can be written as

$$\frac{\partial \boldsymbol{U}}{\partial t} + \operatorname{div} F(\boldsymbol{U}) = B(\boldsymbol{U}) \tag{5}$$

Fig. 4. Comparison between analytical solution and computed results for (*a*) flow height and (*b*) velocity at $t = 0.5$ s. [Colour online.]

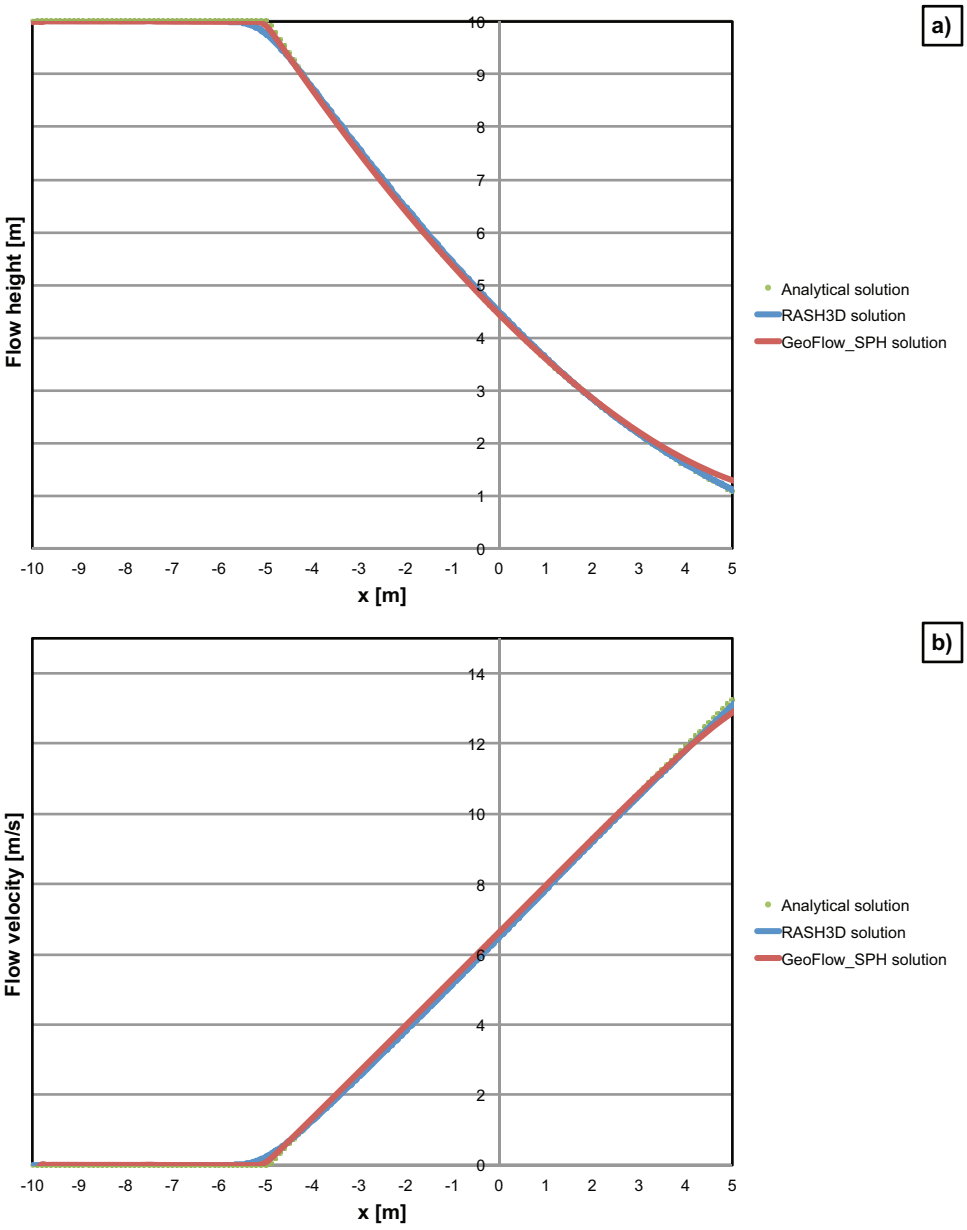

where

$$\boldsymbol{U} = \begin{pmatrix} h \\ hv_x \\ hv_y \end{pmatrix}$$

$$F(\boldsymbol{U}) = \begin{pmatrix} hv_x & hv_y \\ hv_x^2 + \dfrac{g_z h^2}{2} & hv_x v_y \\ hv_x v_y & hv_y^2 + \dfrac{g_z h^2}{2} \end{pmatrix}$$

$$B(\boldsymbol{U}) = \begin{pmatrix} 0 \\ g_x h + \dfrac{1}{\rho} T_x \\ g_y h + \dfrac{1}{\rho} T_y \end{pmatrix}$$

The system of equations is then discretized on an unstructured triangular mesh with a finite element data structure using a particular control volume, which is the median dual cell (Pirulli 2005). Dual cells C_i are obtained by joining the centres of mass of the triangles surrounding each vertex P_i of the mesh (Fig. 1).

For each point P_i of the mesh, the code gives as output the values in time of flow height, velocity in x and y directions, and the maximum values of the height and velocity reached during the whole process up to final deposition of the mass.

Under these hypotheses, the finite volume scheme is written as

$$U_i^{n+1} = U_i^n - \sum\nolimits_{j \in K_i} \frac{\Delta t L_{ij}}{|C_i|} F\left(U_i^n, U_j^n, n_{ij}\right) + \Delta t B\left(U_i^n\right) \quad (6)$$

where U_i^{n+1}, U_i^n is the approximation of the cell average of the exact solution $\boldsymbol{U}$ for the ith cell, at times t^n and t^{n+1}, respectively; and K_i is the set of nodes P_j surrounding P_i. $F(U_i^n, U_j^n, n_{ij})$ denotes an inter-

Fig. 5. Frictional dam break problem on inclined plane. [Colour online.]

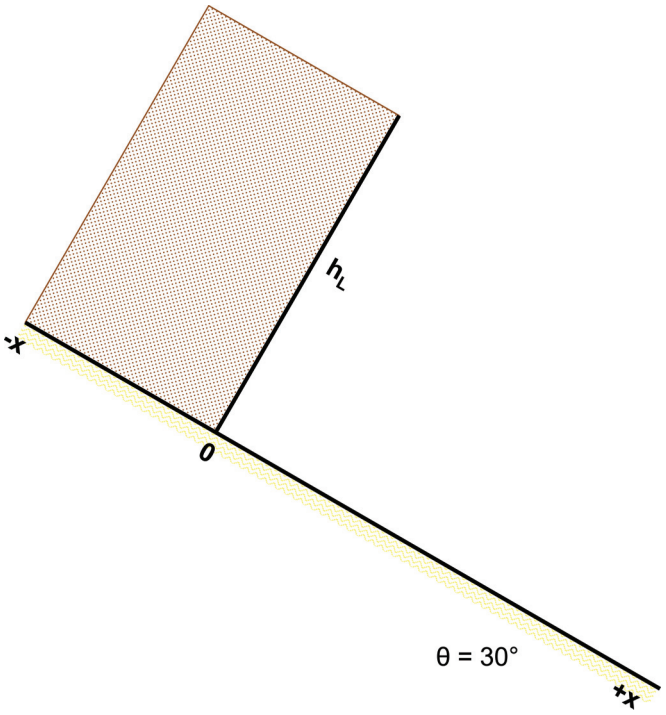

polation of the normal component of the flux $F(\boldsymbol{U})\cdot n_{ij}$ along boundary edge Γ_{ij}, with length L_{ij}, which separates cells C_i and C_j (Fig. 1), Δt is the time step, $|C_i|$ is the area of C_i, $B(U_i^n)$ is the approximation of the ith cell average of the exact source term, $B(\boldsymbol{U})$, at time t^n (Audusse et al. 2000). The summation sign in the second term of the right hand side of eq. (6) indicates that the computation here includes all the boundary edges of the considered ith cell. In RASH3D, a proper calculation of the projection of the term of gravity in the equations that form eq. (3) is obtained, for a finite volume method and a complex topography, by computing the line of maximum dip of each cell, projecting it on the plane tangent to the topography, and re-projecting the obtained direction on the x and y axes of the reference system (Pirulli 2005).

3.2. GeoFlow_SPH model

The GeoFlow_SPH model proposed by Pastor et al. (2009) is based on the theoretical framework of Hutchinson (1986) and Pastor et al. (2002) and it schematizes the propagating mass as a one-phase mixture of solid particles and water. The governing equations (eq. (3)) are solved using the SPH model (Lucy 1977; Gingold and Monaghan 1977).

In the SPH model, a given function, $\phi(x)$, and its spatial derivatives can be approximated by integral approximations defined in terms of kernel and they can be further approximated by replacing them with summations over all the corresponding values at the neighbouring particles in a local domain.

The following equality is the starting point of SPH approximation:

$$\langle\phi(x)\rangle = \int_{\Omega} \phi(x')W(x' - x, l)\, dx' \tag{7}$$

where $\langle\phi(x)\rangle$ is the integral approximation of $\phi(x)$, Ω is the integration domain, $W(x' - x, l)$ is the smoothing kernel function, and l is the smoothing length defining the influence area of W.

The accuracy of the numerical solution and the level of approximation for engineering purposes are a function of the properties and dimensions of the kernel W. In particular, the smoothing kernel function W has to satisfy three main properties: (*i*) its integration returns the unity, (*ii*) when l tends to zero, the kernel function is the Dirac delta function, and (*iii*) when $|x' - x| > kl$, with k a constant that defines the effective area of the smoothing function, W is equal to 0. The latter condition guarantees that the integration over the entire problem domain is localized over the support domain of the smoothing function, which coincides with Ω.

Equation (7) is valid at the continuum level; because, in the problem concerning the propagation of a rapid landslide, the information is stored in a discrete framework (e.g., in a series of nodes), the SPH kernel approximation is converted to discretized forms. Thus, the propagating mass is discretized through a set of moving "particles" or "nodes" in which regular distributions are used to approximate the values of functions and derivatives. Each node, i, has the following nodal variables: h is the height of the landslide, $\bar{\boldsymbol{v}}$ is the depth-averaged velocity, $\boldsymbol{T}^{\mathrm{b}}$ is the surface vector force at the bottom, m is a fictitious mass defined as Ωh, $\bar{p}$ is the averaged pressure term (= $(1/2)b_3h^2$), and $\bar{\boldsymbol{\sigma}}^*$ is the depth-averaged modified stress tensor equal to $\bar{\sigma} + \bar{p}\delta$.

Consequently, eq. (7) can be rewritten as follows:

$$\langle\phi(x_i)\rangle = \sum_{j=1}^{N} \frac{m_j}{\rho_j}\phi(x_j)W_{ij} \tag{8}$$

where ρ_j is the fictitious density of the particle j, N is the number of nodes, and W_{ij} is the value of smoothing kernel defined as $W(x_j - x_i, h)$. Summarizing, the integral approximation of a function $\phi(x)$ at the node i is defined as the sum of the function values estimated at the nodes j, included in the support domain Ω (Fig. 2).

Under these hypotheses, the system of equations that form eq. (3) can be rewritten as

$$\frac{\bar{d}h_i}{dt} = h_i \sum_j \frac{m_j}{h_j} v_{ij}\, \mathrm{grad}W_{ij} \tag{9}$$

$$\frac{\bar{d}}{dt}\bar{v}_l = -\sum_j m_j\left(\frac{\bar{p}_i}{h_i^2} + \frac{\bar{p}_j}{h_j^2}\right)\mathrm{grad}W_{ij} + \frac{1}{\rho}\sum_j m_j\left(\frac{\bar{\sigma}_i^*}{h_i^2} + \frac{\bar{\sigma}_j^*}{h_j^2}\right)\mathrm{grad}W_{ij} + b + \frac{1}{\rho h_i}|N^{\mathrm{B}}|T_i^{\mathrm{B}} \tag{10}$$

where v_{ij} is the difference between v_i and v_j and $|N^{\mathrm{B}}| = \left(\frac{\partial Z^2}{\partial x_1} + \frac{\partial Z^2}{\partial x_2} + 1\right)^{\frac{1}{2}}$ with Z being the height of the basal surface.

In GeoFlow_SPH code, eqs. (9) and (10) are discretized in time with the explicit scheme of fourth order Runge Kutta. As in RASH3D, the terrain information are given by DEM; to allow searching neighbour particles, an auxiliary temporary structured grid, defined by the minimum smoothing length, covering the part of the terrain covered by SPH particles is used (Fig. 2).

The outputs of the code are the values of velocity and depositional height evaluated at each time step.

A detailed description of the method can be found in Pastor et al. (2015).

3.3. Dam break: comparison between numerical and analytical results

This section is devoted to present a benchmark for comparing the predictive capability of the two codes. When numerical models are employed, it is fundamental to know the accuracy of numerical results by performing analyses on cases that have ana-

Fig. 6. Comparison between analytical solution and computed results for (*a*) flow height and (*b*) velocity at t = 30 s. [Colour online.]

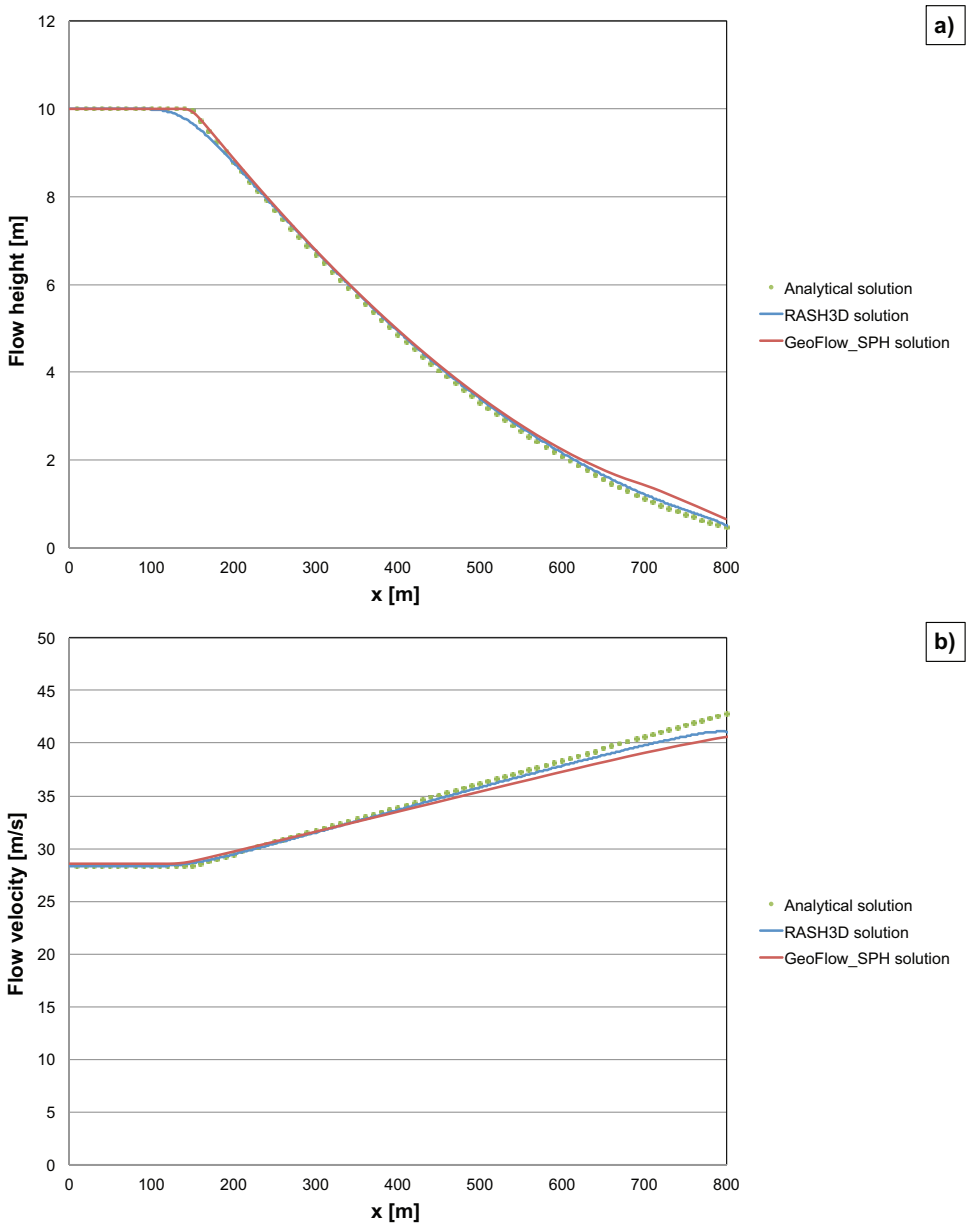

lytical solutions. This is the case of a one-dimensional (1D) dam break problem where a vertical wall retaining water suddenly collapses (Fig. 3). The propagation domain is assumed dry; that is, there is no water at the right side of the wall before the collapse. Moreover, no internal and basal friction and viscous effects are considered.

The initial height condition is given by the piecewise constant function

$$h(x,0) = \begin{cases} h_L & \text{if } x \le 0 \\ 0 & \text{if } x > 0 \end{cases} \tag{11}$$

and the velocity by

$$u(x,0) = 0 \tag{12}$$

where h_L is the initial height equals to 10 m.

The analytical solutions (Stoker 1957; Guinot 2003) for a 1D dam break problem under the hypothesis of a dry, frictionless bed are

$$h(x,t) = \begin{cases} h_L & \text{if } x \le -2\sqrt{gh_L}t \\ \frac{1}{9g}\left(2\sqrt{gh_L} - \frac{x}{t}\right)^2 & \text{if } -2\sqrt{gh_L}t < x \le 2\sqrt{gh_L}t \\ 0 & \text{if } x > 2\sqrt{gh_L}t \end{cases} \tag{13}$$

$$u(x,t) = \begin{cases} 0 & \text{if } x \le -\sqrt{gh_L}t \\ \frac{2}{3}\left(\sqrt{gh_L} + \frac{x}{t}\right) & \text{if } -\sqrt{gh_L}t < x \le 2\sqrt{gh_L}t \\ 0 & \text{if } x > 2\sqrt{gh_L}t \end{cases} \tag{14}$$

Figure 4 shows the comparison between analytical (green dotted line) and numerical results obtained with RASH3D (blue line) and Geoflow_SPH (red line) codes, in terms of flow height (Fig. 4*a*)

Fig. 7. Location of Nora basin (Orco River valley) in Italy. [Colour online.]

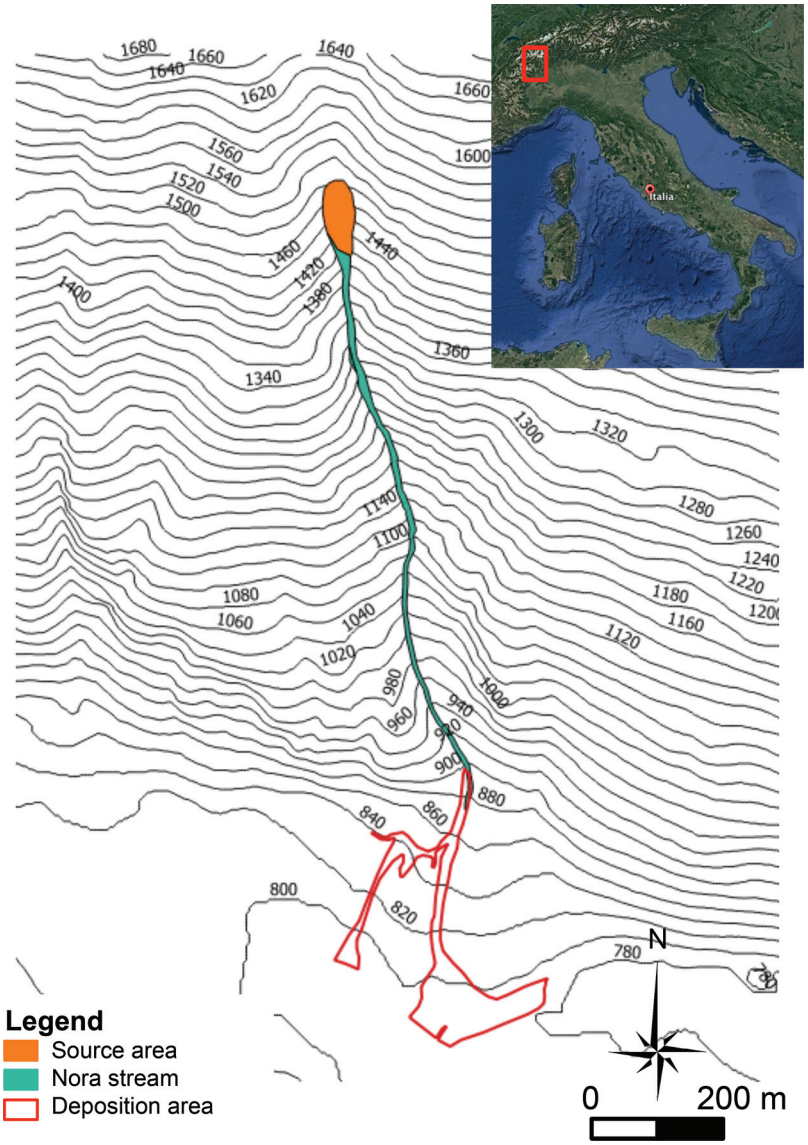

Fig. 8. Deposition area and debris thickness distribution of October 2000 Nora debris flow. [Colour online.]

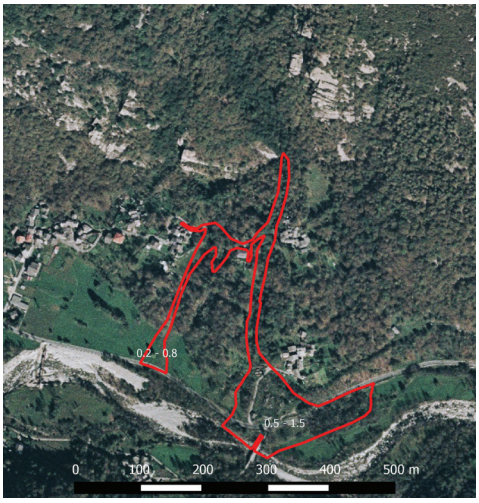

and velocity (Fig. 4*b*) at $t = 0.5$ s. A good agreement between analytical and numerical solutions for each code is found. For what concerns Geoflow_SPH, its computed solution shows a good approximation of the analytical solution, especially in the initiation phase of the flow propagation whereas it overestimates flow height (and consequently it underestimates the velocity) during the rarefaction phase. On the contrary, RASH3D solution presents smoother results in the initiation phase (and consequently it there overestimates the velocity), but a good agreement at the flow front.

3.4. Frictional dam break on slope: comparison between numerical and analytical results

In the previous section, the prediction capability of the two codes was evaluated solving the 1D problem of the collapse of a vertical wall retaining water and comparing the results with the analytical solution presented by Stoker (1957) and Guinot (2003). As the two codes are intended for use with granular material, the case of a frictional fluid behind a dam on a slope is here considered (Fig. 5). Comparing this benchmark with that presented in Section 3.3 “Dam break: comparison between numerical and

Fig. 9. Comparison between (*a*) RASH and (*b*) GeoFlow_SPH propagation path (deposition values) at end of numerical simulation carried out using Voellmy rheology with $\mu = 0.1$ and $\xi = 200$ m/s^2. [Colour online.]

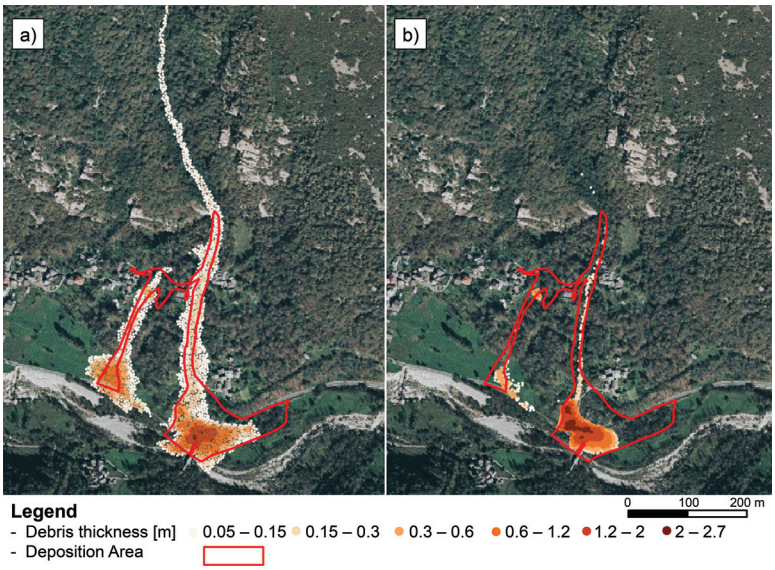

Fig. 10. RASH3D (left) and GeoFlow_SPH (right) simulation at different time steps using same rheological parameters. The two simulations show differences both in term of velocity (flow simulated using SPH is faster) and shape (RASH3D shows a larger lateral spreading). [Colour online.]

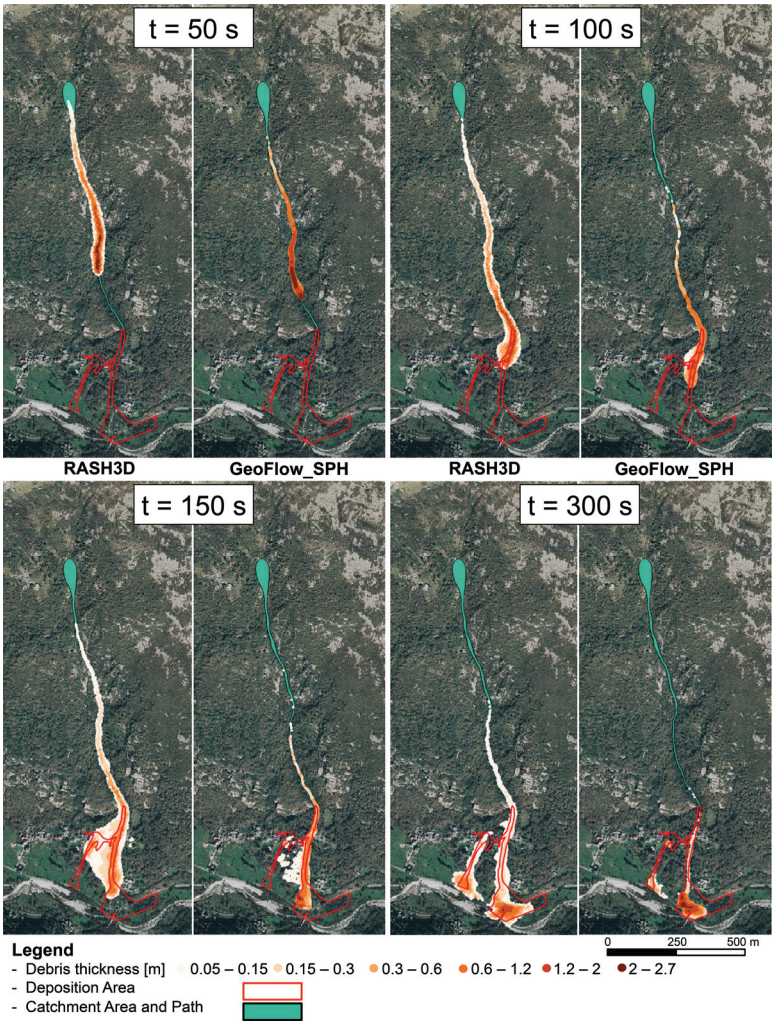

Fig. 11. Comparison of the two numerical code results in terms of velocity differences at (*a*) time step equal to 50 s and (*b*) velocity values obtained during whole simulation. [Colour online.]

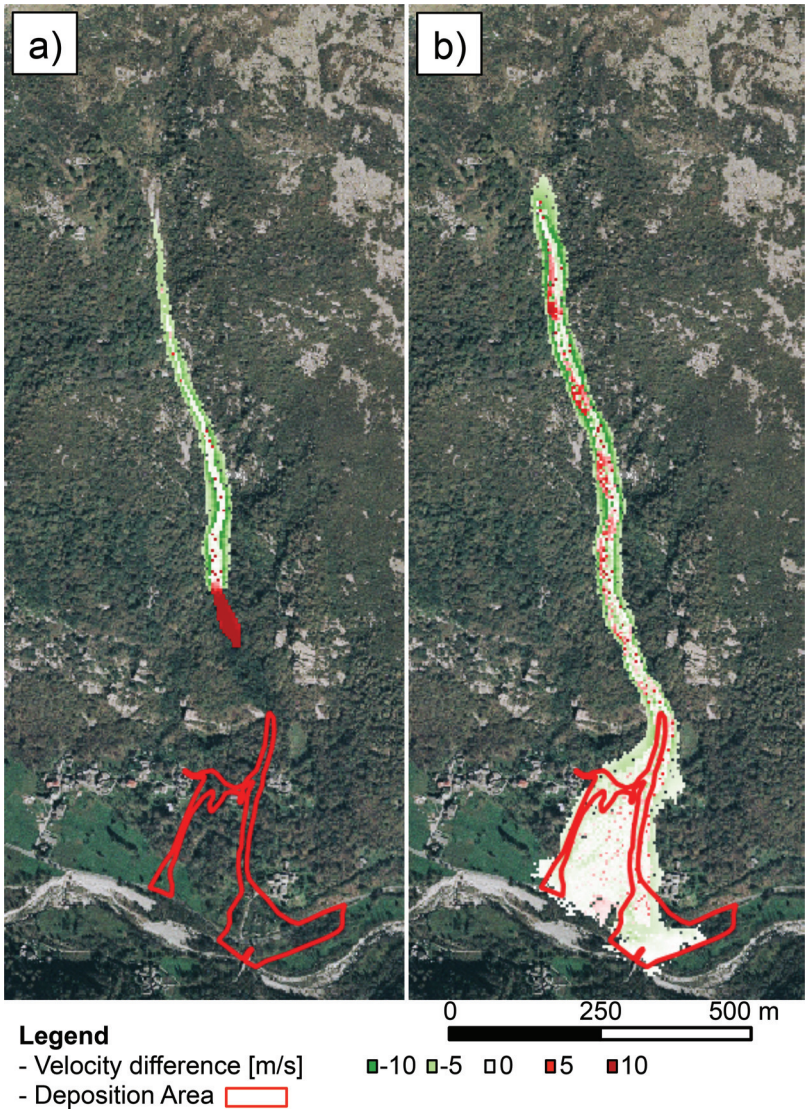

Fig. 12. Back-calculated GeoFlow_SPH final deposit using Voellmy rheology with $\mu = 0.08$ and $\xi = 100$ m/s^2. [Colour online.]

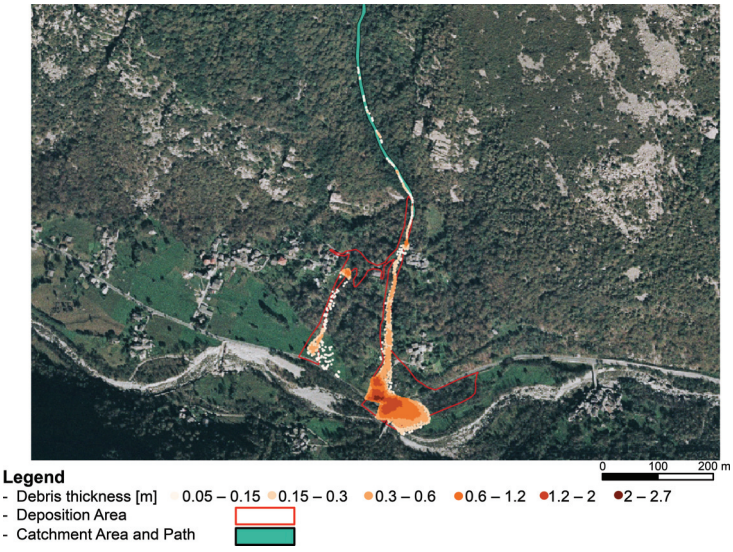

Fig. 13. Comparison between RASH3D (left) and GeoFlow_SPH (right) simulation at different time steps using Voellmy rheology with $\mu = 0.1$ and $\xi = 200$ m/s^2 and $\mu = 0.08$ and $\xi = 100$ m/s^2 respectively. [Colour online.]

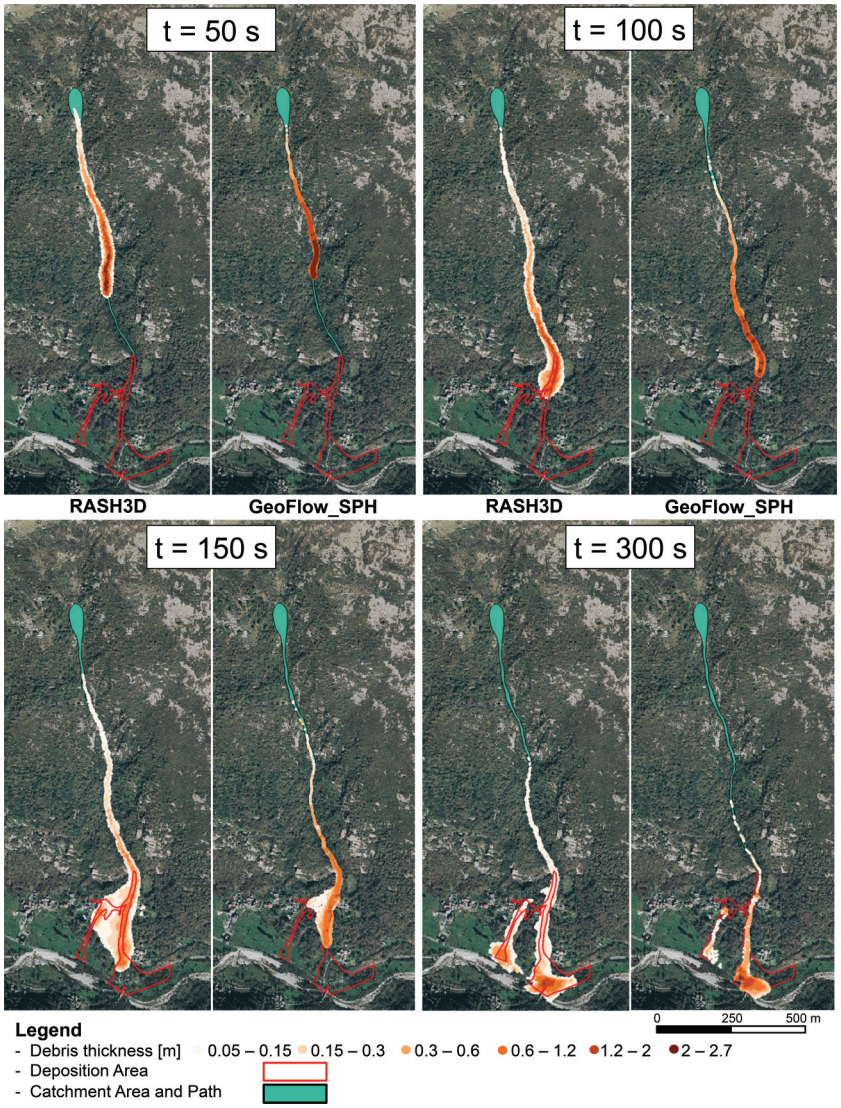

analytical results", there are two additional terms, originated by the slope and the basal friction.

The analytical solution used here to validate the RASH3D and GeoFLow_SPH results was developed by Mangeney et al. 2000 and it allows to easily calculate the flow height and depth-averaged flow velocity for a given time (t) as follows:

$$h(t) = \frac{1}{9g\cos\theta}\left(2c_0 - \frac{x}{t} + \frac{1}{2}mt\right)^2 \quad (15)$$

$$u(t) = \frac{1}{3}\left(2c_0 + \frac{2x}{t} - mt\right) + mt \quad (16)$$

where g is gravitational acceleration, θ is the slope equals to 30°, and the physical quantities c_0 and m are given by the following equations:

$$c_0 = \sqrt{gh_L\cos\theta} \quad (17a)$$

$$m = g\cos\theta\,(\tan\phi - \tan\theta) \quad (17b)$$

where h_L is the initial fluid height and ϕ is the bulk friction angle equal to 10 m and 25°, respectively.

Equations (15) and (16) are valid outside the region defined by $x > -c_0t + (1/2)mt^2$, where the fluid height and the velocity are constant and equal to h_L and mt, respectively, and upstream from the front of the fluid ($h = 0$ and $u = mt$) defined by $x > 2c_0t + (1/2)mt^2$.

In Fig. 6, the comparison between analytical (green dotted line) and numerical results obtained with RASH3D (blue line) and Geoflow_SPH (red line) codes is shown. As in the water dam break case, a good agreement between analytical and numerical solutions for each code was found. For what concerns flow height, the Geoflow_SPH solution presents smoother height values in the initiation phase and a moderate overestimation of the front thickness. RASH3D accentuates the effects of smoothing in the initiation phase, but it shows a negligible overestimation of the front thickness values compared to the analytical solution.

About depth-averaged velocity, it has an opposite trend compared to the height flow: in fact, where simulated thickness values are smaller than analytical ones, simulated velocity values are higher and vice-versa. For these reasons, the main differences between numerical and analytical solutions increase closer to the front flow.

The benchmarks here proposed were used to assess the validity of the discretization technique presented. Others validation exercises can be found in Pastor et al. 2009, 2014, 2015 and Pirulli 2005.

Fig. 14. Differences between maximum velocity values evaluated during whole simulation using Geoflow_SPH and RASH3D best-fit rheological parameters. [Colour online.]

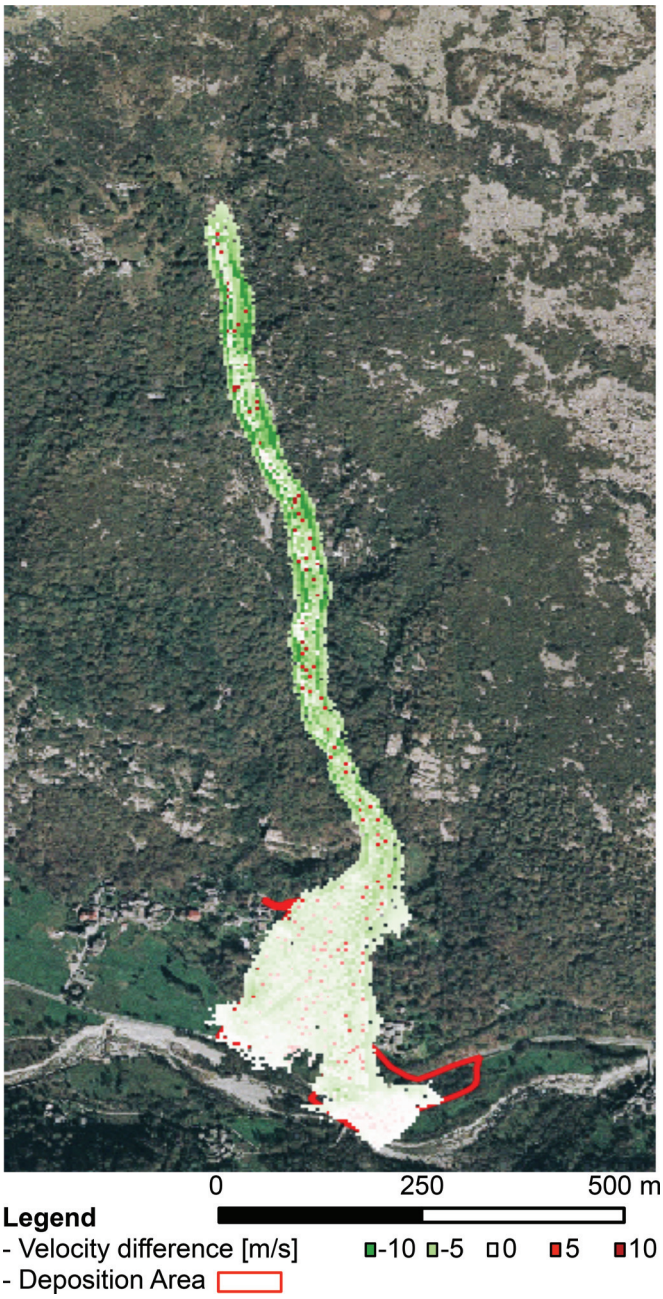

4. Case study: October 2000 Nora debris flow

The Nora stream basin (Fig. 7), a tributary of the Orco River (Piedmont region, Northwestern Alps, Italy), was affected in October 2000 by intense rainfall (the average rainfall value was 400 mm in 60 h, with peak rainfall intensity of 28 mm/h) that caused the formation of a debris slide (ARPA Piemonte 2003). Due to the steep drainage network, the intense surface runoff, and the altered gneissic bedrock, the debris slide rapidly transformed into a channelized noncohesive debris flow (Pirulli and Marco 2010). Although residual pockets of debris located along the channel were re-mobilized, due to their smaller volumes then main moving mass, the entrainment of material during runout can be neglected.

Reaching the fan apex, the debris split into two main branches (Fig. 8), one on the orographic left with thickness values ranging from 0.5 and 1.5 m; the other, on the orographic right with thickness varying between 0.2 and 0.8 m.

After post-event observations (in both the source zone and the depositional areas) and comparison between ground profile pre- and post-event, the bulk debris volume was estimated at approximately 10 000 m^3.

5. Discussion

Do different numerical codes that implement the same governing equations (eq. (3)), but with fundamentally different numerical solvers, give same results or not? Are the differences relevant? What are the consequences concerning the design of potential structural countermeasures?

To answer these questions, in the present section the comparison of results coming from analyses performed using the two numerical codes presented in the preceding paragraph are shown.

The Nora event was already studied and back-analysed with the RASH3D code by Pirulli and Marco (2010). The best-fit numerical simulation was obtained using a 5 m grid spacing DEM and considering a Voellmy rheology with $\mu = 0.1$ and $\xi = 200$ m/s^2.

Note that in contrast with finite difference methods, where pointwise values are approximated, and finite element methods, where basis functions are approximated, in a finite volume method, which is used in RASH3D, the unknowns approximate the average of the solution over the domain grid cell.

Starting from these results, the same analysis, keeping unchanged the rheological parameter values, was carried out using GeoFlow_SPH code. As already mentioned, the meshless particle codes, as GeoFlow_SPH, do not required fixed grid and all of the calculations are performed directly at the particle-centred location. Despite this, beside the 5 m topographic mesh (which provides the topography of the problem), GeoFlow_SPH requires that a secondary grid is used for the debris flow source area definition. In the Rio Nora case, the authors assumed a 1 m spacing secondary grid and consequently a source area made of 212 points was obtained. The smoothing length was set to 2 m.

The topographic mesh resolution for the RASH3D code and the secondary grid resolution and dimension of the smoothing length for GeoFlow_SPH have (considering the same computational power) a great weight on the computational time. For the Rio Nora case, the computational time of GeoFlow_SPH code (5 m spacing topography grid, 1 m spacing secondary grid) is lower than RASH3D one (5 m spacing topography grid), as the computations are made on a set of arbitrarily distributed particles (secondary mesh), which are not connected with fixed grid (topography mesh). In particular, using the same workstation, GeoFlow_SPH computation time is less than 20 times with respect to RASH3D.

In Fig. 9, significant differences can be observed between GeoFlow_SPH and RASH3D simulation especially within the depositional area. In particular,

- GeoFlow_SPH overestimates the depositional thickness values with respect to the RASH3D code. It results a zone located at the orographic left of the deposition area where the depositional height reaches 2.7 m (the maximum on site measured depositional height was 1.5 m).
- GeoFlow_SPH simulation does not reach a satisfactory approximation of the depositional area shape.

Furthermore, analysing the flowing path at different time step (Fig. 10), it is possible to notice that

- At a given time, the travel distance computed with GeoFlow_SPH is greater than that evaluated with RASH3D code. This means that, being equal the rheological parameter values, the flow simulated in GeoFlow_SPH is faster.

Table 1. Comparison between numerical results at apex of alluvial fan calculated using RASH3D and GeoFlow_SPH using the same rheological law (Voellmy with $\mu = 0.1$ and $\xi = 200$ m/s^2).

Code	v_{max} (m/s)	h_{max} (m)
RASH3D	8.76	2.04
GeoFlow_SPH	9.57	2.05

- RASH3D simulation evidences a pronounced lateral spreading of the flowing mass.

Figure 11 shows the differences between velocity values obtained using GeoFlow_SPH and RASH3D at the same time step (Fig. 11*a*) and the differences between maximum velocity values reached during the whole simulation (Fig. 11*b*). Analysing Fig. 11*a*, the aforementioned observations are confirmed. It is in fact possible to notice that the positive variation of velocity (dark red color) corresponds to the front of the GeoFlow_SPH simulated flow; on the contrary, the negative variation (dark green) marks the lateral spreading of the RASH3D simulation. Differences between calculated velocities are not appreciable (<5 m/s) within the flow body. Concerning the variation of maximum calculated velocities (Fig. 11*b*), it is interesting to underline that the most significant differences are in the upper part of the stream, where the channel is steeper, whereas in correspondence of the alluvial fan there are only appreciable differences between evaluated velocity at the boundary of the deposition area.

Other simulations were run to also find the best-fit between depositional area and GeoFlow_SPH results. The best correspondence between depositional height and spatial distribution of the deposit was obtained with $\mu = 0.08$ and $\xi = 100$ m/s^2 (Fig. 12).

Comparing the numerical results of the two calibrated codes, Fig. 13 evidences a good correspondence between the numerically calculated depositional height and in situ surveyed deposit thickness distribution. It is possible, in particular to notice that

- The shape of the flowing mass is slightly different for the two codes: in RASH3D, a pronounced lateral spreading along the channel is evident. Furthermore, RASH3D flow shows a greater elongation compared to the GeoFlow_SPH simulated flowing mass.
- In this case, GeoFlow_SPH velocities are slower than those of RASH3D.

Analysing the variation of the maximum velocity values computed using the two codes and their best-fit rheological parameters (Fig. 14), it is clear that, along the simulated flow path, there are no relevant differences, especially in the depositional area (velocity differences vary between −5 and 5 m/s). The most relevant difference is observed along the boundary of the run out path. RASH3D overestimates the lateral spreading of the flow with respect to GeoFlow_SPH. This aspect also emerges in the most compact configuration of the GeoFlow_SPH deposit with respect to RASH3D.

The fact that the rheological parameter values are not interchangeable, from an engineering point of view, has relevant consequences. For instance, hypothesizing the construction of a protection structure at the apex point of the alluvial fan (e.g., Fig. 7), it is evident that numerical GeoFlow_SPH velocity is about 10% greater than that calculated using RASH3D best-fit rheological values (Table 1). Instead, there are no differences between the values of maximum flow height.

6. Conclusions

The two codes RASH3D and GeoFlow_SPH, based on a continuum mechanics approach, were used to back-analyse the debris flow event that occurred in October 2000 at the Nora basin, northwestern Italian Alps.

The presented back-analysis evidences that both modelling of past debris flow events and forecasting of future scenarios require to understand and quantify the result discrepancy generated by the use of different numerical codes. The analyses carried out in this paper clearly show that, even if a rheology is selected to back-analyse the same case study with different codes, the obtained calibrated values of rheological parameters are not interchangeable among the codes. This fact has important consequences in the definition of risk scenarios or for planning debris flow countermeasures.

Summarizing, the uncertainties related to evaluation of propagation characteristics are consequences of both choice of the numerical code and rheological parameter values. This is a key point that has to be taken into account by practicing engineers that use codes rather than produce them.

Concerning the analysed case, it emerges that

- Adopting the same rheological parameter values the two codes give different areal depositional distribution and different velocity and thickness values.
- RASH3D code always gives a larger lateral mass spreading with respect to GeoFlow_SPH.
- To obtain comparable results in terms of depositional height distribution, the best combination of rheological parameters for GeoFlow_SPH is $\mu = 0.08$ and $\xi = 100$ m/s^2.
- The main differences between the two codes are related to velocity values (the GeoFlow_SPH velocity value results 10% greater than the RASH3D ones, by using RASH3D best fit rheological values). No significant differences between maximum depth values are emerged.

References

ARPA Piemonte. 2003. Eventi alluvionali in Piemonte. Evento alluvionale regionale del 13–16 ottobre 2000. Agenzia Regionale per la Protezione Ambientale (ARPA) Piemonte, Turin, Italy.

Audusse, E., Bristeau, M.O., and Perthame, B. 2000. Kinetic schemes for Saint-Venant equations with source terms on unstructured grids. Institut National de Recherche en Informatique et Automatique, LeChesnay, France. Rapport de Recherche, No. 3989, pp. 1–44.

Cannon, S.H. 1993. An empirical model for the volume-change behaviour of debris flows. *In* Proceedings of ASCE National Conference On Hydraulic Engineering, San Francisco, California, July 25–30, pp. 1768–1773.

Cascini, L., Cuomo, S., Pastor, M., Sorbino, G., and Piciullo, L. 2014. SPH run-out modelling of channelised landslides of the flow type. Geomorphology, **214**: 502–513. doi:10.1016/j.geomorph.2014.02.031.

Corominas, J. 1996. The angle of reach as a mobility index for small and large landslides. Canadian Geotechnical Journal, **33**(2): 260–271. doi:10.1139/t96-005.

Cuomo, S., Pastor, M., Cascini, L., and Castorino, G.C. 2014. Interplay of rheology and entrainment in debris avalanches: a numerical study. Canadian Geotechnical Journal, **51**(11): 1318–1330. doi:10.1139/cgj-2013-0387.

Dutto, P., Stickle, M.M., Pastor, M., Manzanal, D., Yague, A., Tayyebi, S., Lin, C., and Elizaide, M.D. 2017. Modelling of fluidised geomaterials: the case of the Aberfan and the gypsum tailings impoundment flowslides. Materials, **10**: E562. doi:10.3390/ma10050562. PMID:28772924.

Gingold, R.A., and Monaghan, J.J. 1977. Smoothed particle hydrodynamics: theory and application to non-spherical stars. Monthly Notices of the Royal Astronomical Society, **181**(3): 375–389. doi:10.1093/mnras/181.3.375.

Gray, J.M.N.T., Wieland, M., and Hutter, K. 1999. Gravity-driven free surface flow of granular avalanches over complex basal topography. Proceedings of the Royal Society of London, Series A, Mathematical, Physical, and Engineering Sciences **455**(1985). doi:10.1098/rspa.1999.0383.

Guinot, V. 2003. Godunov-type schemes. An introduction for engineers. Elsevier, Amsterdam.

Hungr, O. 1995. A model for the runout analysis of rapid flow slides, debris flows, and avalanches. Canadian Geotechnical Journal, **32**(4): 610–623. doi:10.1139/t95-063.

Hungr, O., and Evans, S.G. 1996. Rock avalanche runout prediction using a dynamic model. *In* Proceedings of the 7th International Symposium on Landslides, 17–21 June 1996, Trondheim. *Edited by* K. Senneset. A.A. Balkema, Rotterdam. Vol. 1, pp. 233–238.

Hutchinson, J.N. 1986. A sliding–consolidation model for flow slides. Canadian Geotechnical Journal, **23**(2): 115–126. doi:10.1139/t86-021.

Iverson, R.M., and Denlinger, R.P. 2001. Flow of variably fluidized granular masses across three-dimensional terrain: 1. Coulomb mixture theory. Journal of Geophysical Research: Solid Earth, **106**(B1): 537–552. doi:10.1029/2000JB900329.

Jakob, M., and Hungr, O. 2005. Debris-flow hazards and related phenomena. Springer-Verlag, Berlin.

Lucy, L.B. 1977. A numerical approach to the testing of the fission hypothesis. The Astronomical Journal, **82**: 1013. doi:10.1086/112164.

Mangeney, A., Heinrich, P., and Roche, R. 2000. Analytical solution for testing debris avalanche numerical models. Pure Applied Geophysics, **157**: 1081–1096. doi:10.1007/s000240050018.

Mangeney-Castelnau, A., Vilotte, J.-P., Bristeau, M.O., Perthame, B., Bouchut, F., Simeoni, C., and Yernini, S. 2003. Numerical modelling of avalanches based on Saint-Venant equations using a kinetic scheme. Journal of Geophysical Research, Solid Earth, **108**(B11): 1–18. doi:10.1029/2002JB002024.

Manzella, I., Pirulli, M., Naaim, M., Serratrice, J.F., and Labiouse, V. 2008. Numerical modelling of a rock avalanche laboratory experiment in the framework of the "Rockslidetec" alpine project. *In* Landslides and Engineered Slopes: Proceedings of the 10th International Symposium on Landslides and Engineered Slopes. *Edited by* Chen Z. et al.; Xi'an, Cina, 30 Giugno - 4 Luglio 2008, Taylor & Francis Group, London, Vol. 1, pp. 835–841.

McDougall, S., and Hungr, O. 2005. Dynamic modelling of entrainment in rapid landslides. Canadian Geotechnical Journal, **42**(5): 1437–1448. doi:10.1139/t05-064.

O'Brien, J.S., Julien, P.Y., and Fullerton, W.T. 1993. Two-dimensional water flood and mudflow simulation. Journal of Hydraulic Engineering, **119**(2): 244–261. doi:10.1061/(ASCE)0733-9429(1993)119:2(244).

Pastor, M., Quecedo, M., Merodo, J.A.F., Herrores, M.I., González, E., and Mira, P. 2002. Modelling tailings dams and mine waste dumps failures. Géotechnique, **52**(8): 579–591. doi:10.1680/geot.2002.52.8.579.

Pastor, M., Blanc, T., Pastor, M.J., Sanchez, M., Haddad, B., Mira, P., Fernandez Merodo, J.A., Herreros, I., and Drempetic, V. 2007. A SPH depth integrated model with pore pressure coupling for fast landslides and related phenomena. *In* Proceedings of the 2007 International Forum on Landslide Disaster Management. *Edited by* K. Ho and V. Li., Hong Kong, 10–12 December 2007, Vol. II, pp. 987–1014.

Pastor, M., Haddad, B., Sorbino, G., Cuomo, S., and Drempetic, V. 2009. A depth-integrated, coupled SPH model for flow-like landslides and related phenomena. International Journal for Numerical and Analytical Methods in Geomechanics, **33**(2): 143–172. doi:10.1002/nag.705.

Pastor, M., Haddad, V., Mira, P., and Fernandez-Merodo, J.A. 2014. Depth averaged models for rock avalanche propagation: an SPH approach. *In* Rock Slope Stability 2014, Marrakesh, Morocco, 2–4 April 2014, pp. 35–58.

Pastor, M., Blanc, T., Haddad, B., Drempetic, V., Morles, M.S., Dutto, P., Stickle, M.M., Mira, P., and Fernández Merodo, J.A. 2015. Depth averaged models for fast landslide propagation: mathematical, rheological and numerical aspects. Archives of Computational Methods in Engineering, **22**: 67–104. doi:10.1007/s11831-014-9110-3.

Pirulli, M. 2005. Numerical modelling of landslide runout, a continuum mechanics approach. Ph.D. dissertation, Politecnico of Turin, Turin, Italy.

Pirulli, M. 2009. The Thurwieser rock avalanche (Italian Alps): Description and dynamic analysis. Engineering Geology, **109**(1–2): 80–92. doi:10.1016/j.enggeo.2008.10.007.

Pirulli, M. 2016. Numerical simulation of possible evolution scenarios of the Rosone deep-seated gravitational slope deformation (Italian Alps, Piedmont). Rock Mechanics and Rock Engineering, **49**(6): 2373–2388. doi:10.1007/s00603-015-0857-0.

Pirulli, M., and Marco, F. 2010. Description and numerical modelling of the October 2000 Nora debris flow, Northwestern Italian Alps. Canadian Geotechnical Journal, **47**(2): 135–146. doi:10.1139/T09-082.

Pirulli, M., and Pastor, M. 2012. Numerical study on the entrainment of bed material into rapid landslides. Géotechnique, **62**(11): 959–972. doi:10.1680/geot.10.P.074.

Pirulli, M., and Scavia, C. 2007. A set of benchmark tests to assess the performance of a continuum mechanics depth-integrated model. *In* Proceedings of the 2007 International Forum on Landslide Disaster Management. *Edited by* K. Ho and V. Li, Hong Kong, 10–12 December 2007, Vol. II, pp. 1015–1042.

Pirulli, M., and Sorbino, G. 2008. Assessing potential debris flow runout: a comparison of two simulation models. Natural Hazards and Earth System Science, **8**(4): 961–971. doi:10.5194/nhess-8-961-2008.

Pirulli, M., Barbero, M., Marchelli, M., and Scavia, C. 2017. The failure of the Stava Valley tailings dams (Northern Italy): numerical analysis of the flow dynamics and rheological properties. Geoenvironmental Disasters, **4**: 3. doi:10.1186/s40677-016-0066-5.

Pisani, G., Pirulli, M., Labiouse, V., and Scavia, C. 2013. Influence of bed curvature on the numerical modelling of unconstrained granular materials. *In* Landslide Science and Practice. Vol. 3: Spatial Analysis and Modelling; *Edited by* C. Margottini, P. Canuti, and K. Sassa. Springer, Berlin, pp. 271–276.

Pouliquen, O. 1999. Scaling laws in granular flows down rough inclined planes. Physics of Fluids, **11**(3): 542–548. doi:10.1063/1.869928.

Revellino, P., Hungr, O., Guadagno, F.M., and Evans, S.G. 2004. Velocity and runout simulation of destructive debris flows and debris avalanches in pyroclastic deposits, Campania region, Italy. Environmental Geology, **45**(3): 295–311. doi:10.1007/s00254-003-0885-z.

Rickenmann, D. 1999. Empirical relationships for debris flows. Natural Hazards, **19**(1): 47–77. doi:10.1023/A:1008064220727.

Rickenmann, D. 2005. Runout prediction methods. Debris-flow hazards and related phenomena. Springer Praxis Books, pp. 305–324.

Rickenmann, D., and Koch, T. 1997. Comparison of debris flow modelling approaches. *In* Proceedings of the 1st International Conference On Debris Flow Hazards Mitigation: Mechanics, Prediction and Assessment, ASCE, Reston, Va., USA, pp. 576–585.

Sauthier, C., Pirulli, M., Pisani, G., Scavia, C., and Labiouse, V. 2015. Numerical modelling of gravel unconstrained flow experiments with the DAN3D and RASH3D codes. Computers & Geosciences, **85**: 81–90. doi:10.1016/j.cageo.2015.09.008.

Savage, S.B., and Hutter, K. 1989. The motion of a finite mass of granular material down a rough incline. Journal of Fluid Mechanics, **199**(1): 177. doi:10.1017/S0022112089000340.

Stoker, J.J. 1957. Water waves. Interscience, New York.

Vagnon, F. 2017. Theoretical and experimental study on the barrier optimization against debris flow risk. Ph.D. dissertation, University of Turin, Turin, Italy.

List of symbols

$B(\boldsymbol{U})$	source term
$B(U_i^n)$	approximation of ith cell average of exact source term, $B(\boldsymbol{U})$, at time t^n
b	bottom elevation in the (x, y, z) coordinate system
C_i	dual cells
$\lvert C_i\rvert$	area of C_i
$F(\boldsymbol{U})$	flux term
$F(U_i^n, U_j^n, n_{ij})$	interpolation of normal component of flux $F(\boldsymbol{U})\cdot n_{ij}$ that separates C_i and C_j
g	gravitational acceleration
$\boldsymbol{g}$	gravitational acceleration vector
H	characteristic flow thickness
h	flow depth
h_L	initial height (fluid)
$h(x, 0)$	constant function for initial height condition
K_i	set of nodes P_j surrounding P_i
k	constant defines effective area of smoothing function
L	characteristic length of flowing mass
L_{ij}	length of boundary edge
l	smoothing length
m	fictitious mass (= Ωh)
$\boldsymbol{n}_b$	unit vector normal to bed
N	number of nodes
P_i	vertex of mesh
$\overline{p}$	averaged pressure term
$\boldsymbol{T}$	traction vector (= (T_x, T_y, T_z))
$\boldsymbol{T}^b$	surface vector force at bottom of flow
T_t	tangential stress
$\lVert T_n\rVert$	norm of normal traction
T_i^B	rheological law at bottom of flow
$\boldsymbol{U}$	velocity vector
U_i^{n+1}, U_i^n	approximation of cell average of exact solution $\boldsymbol{U}$ for ith cell, at times t^n and t^{n+1}, respectively
$u(x, 0)$	constant function for velocity
$\boldsymbol{v}$	flow velocity vector (= (v_x, v_y, v_z))
$\overline{\boldsymbol{v}}$	depth-averaged flow velocity (= $(\overline{v}_x, \overline{v}_y)$)
$\overline{\boldsymbol{v}}_i$	depth-averaged flow velocity in x and y direction
v_{ij}	difference between v_i and v_j
W	kernel of linear function
W_{ij}	value of smoothing kernel (= $W(x_j - x_i, h)$)
Z	height of basal surface
Γ_{ij}	boundary edge
Δt	time step
δ	Dirac delta function
θ	slope
μ	frictional coefficient
ξ	turbulent coefficient
ρ	mass density
ρ_j	fictitious (or simulated) density of particle j
$\sigma(x, y, z, t)$	Cauchy stress tensor
$\overline{\sigma}$	depth-averaged Cauchy stress tensor
$\overline{\boldsymbol{\sigma}}^*$	depth-averaged modified stress tensor (= $\overline{\sigma} + \overline{p}\delta$)
σ_c	upper bound of the admissible stresses
ϕ	bulk friction angle
$\phi(x)$	given function
$\langle\phi(x)\rangle$	integral approximation of given function
Ω	integration domain